JOURNAL OF THE MECHANICAL BEHAVIOR OF BIOMEDICAL MATERIALS 52 (2015) 95–107

Available online at www.sciencedirect.com

ScienceDirect

www.elsevier.com/locate/jmbbm

Research Paper

Teleost fish scales amongst the toughest collagenous materials

A. Khayer Dastjerdi, F. Barthelat*

Department of Mechanical Engineering, McGill University, Montreal, QC, Canada

ARTICLE INFO

Article history:
Received 27 May 2014
Received in revised form
23 September 2014
Accepted 27 September 2014
Available online 6 October 2014

Keywords:
Fish scales
Collagen
Toughness
Process zone
Crack bridging
Bio-inspired materials

ABSTRACT

Fish scales from modern teleost fish are high-performance materials made of cross-plies of collagen type I fibrils reinforced with hydroxyapatite. Recent studies on this material have demonstrated the remarkable performance of this material in tension and against sharp puncture. Although it is known that teleost fish scales are extremely tough, actual measurements of fracture toughness have so far not been reported because it is simply not possible to propagate a crack in this material using standard fracture testing configurations. Here we present a new fracture test setup where the scale is clamped between two pairs of miniature steel plates. The plates transmit the load uniformly, prevent warping of the scale and ensure a controlled crack propagation. We report a toughness of 15 to 18 kJ m^{-2} (depending on the direction of crack propagation), which confirms teleost fish scales as one of the toughest biological material known. We also tested the individual bony layers, which we found was about four times less tough than the collagen layer because of its higher mineralization. The mechanical response of the scales also depends on the cohesion between fibrils and plies. Delamination tests show that the interface between the collagen fibrils is three orders of magnitude weaker than the scale, which explains the massive delamination and defibrillation observed experimentally. Finally, simple fracture mechanics models showed that process zone toughening is the principal source of toughening for the scales, followed by bridging by delaminated fibrils. These findings can guide the design of cross-ply composites and engineering textiles for high-end applications. This study also hints on the fracture mechanics and performance of collagenous materials with similar microstructures: fish skin, lamellar bone or tendons.

1. Introduction

Over millions of years of evolution, biological organisms have developed high-performance natural materials to fulfill a variety of structural functions. Materials like bone, teeth, scales or mollusk shells possess outstanding mechanical properties despite their relatively weak ingredients. During the past decade much research has been devoted to understanding the concepts, structures and mechanisms underlying the performance of these natural materials, so they can be implemented in high performance synthetic materials (Barthelat, 2007; Bonderer et al., 2008; Mayer, 2005; Studart, 2012; Mirkhalaf et al., 2014). Mollusk shells, arthropod cuticles, bone, teeth have already attracted a great deal of

*Corresponding author.
E-mail address: francois.barthelat@mcgill.ca (F. Barthelat).

http://dx.doi.org/10.1016/j.jmbbm.2014.09.025
1751-6161/

attention, and more recently many more natural materials have emerged as potential source of inspiration for new biomimetic materials (Meyers et al., 2008; Dimas and Buehler, 2012; Weaver et al., 2012). The structure and mechanics of natural scaled skin, and more particularly fish scales, have recently been the subject of several studies (Yang et al., 2013a,b; Bruet et al., 2008; Ikoma et al., 2003; Garrano et al., 2012; Lin et al., 2011; Meyers et al., 2012; Zhu et al., 2012, 2013; Browning et al., 2013; Zimmermann et al., 2013; Vernerey and Barthelat, 2010). Since their emergence 500 million year ago, fish have evolved scales with different shapes, sizes and arrangements which are generally classified into cosmoid, ganoid, placoid and elasmoid (Benton, 2004). Over the course of evolution the bony multilayered cosmoid and ganoid categories have largely been replaced by thinner yet more flexible teleost scales (Kardong, 2006). Natural scaled skins have remarkable mechanical properties: compliance, resistance to penetration, lightweight, and ultrathin structure (Yang et al., 2013a,b). Several studies on the structure and mechanics of fish scales were performed since on ancient bony scales (Bruet et al., 2008; Yang et al., 2013a,b) and on the more modern and lighter teleost scales (Ikoma et al., 2003; Garrano et al., 2012; Lin et al., 2011; Zhu et al., 2012). Mechanical characterization typically involved tensile testing (Ikoma et al., 2003; Garrano et al., 2012; Lin et al., 2011; Zhu et al., 2012) or indentation and puncture tests on individual scales (Bruet et al., 2008; Meyers et al., 2012; Zhu et al., 2012) or multiple scales (Zhu et al., 2013). Fish scales have also started to inspire new flexible protective systems (Browning et al., 2013; Chintapalli et al., 2014). Tensile tests on natural teleost fish scales confirmed the scale as a stiff, strong a tough material. In collagenous scales extensive inelastic deformation and energy dissipation were observed including pullout, defibrillation, sliding and rotation (Ikoma et al., 2003; Garrano et al., 2012; Lin et al., 2011; Zhu et al., 2012; Zimmermann et al., 2013). The function of the scaled skin is to provide protection while maintaining high compliance in flexion to allow for motion (Vernerey and Barthelat, 2010). One of the main functions of the scale is therefore mechanical protection against predators, collisions with other fish or obstacles or other mechanical threats. Recent studies have therefore focused on the indentation and puncture resistance of individual scales (Bruet et al., 2008; Zhu et al., 2012), showing that scales are superior to engineering materials such as polycarbonate and polystyrene (Zhu et al., 2012). This high performance can be explained by the ability of the material to dissipate large amounts of energy through large deformations. In turn, these large deformations are possible because the material can resist the propagation of cracks that could emanate from pre-existing defects in the materials and/or from high stress concentrations typical to puncture or laceration. In this context high fracture toughness becomes a desirable property, and early tests noted that indeed some fish scales are so tough that they could not be fractured, even after immersion in liquid nitrogen (Currey, 1999). Fracture tests on nonlinear, extensible and tough materials are in general difficult using traditional fracture testing configurations. For elastomers the "trouser" tear test circumvents some of the experimental difficulties (ASTM, 2003), and it is successfully applied on biological elastomers such as skin (Purslow, 1983). However, this test provides a mode III fracture toughness, which may differ from mode I fracture especially if fracture process is governed by defibrillation and fiber bridging as in fish scales. Instrumented mode I fracture tests on individual fish scales are extremely difficult because of their small size and high fracture toughness. To the best of our knowledge, toughness could only be measured on scales from gar, which are heavy ganoid scales with sufficient size, thickness and stiffness to permit toughness measurement in bending (Yang et al., 2013a,b). Gar scales were found similar to cortical bone in terms of composition, structure and fracture toughness (3 to 5 MPa $m^{1/2}$ (Yang et al., 2013a,b)). However it has so far been impossible to measure the toughness of teleost fish scales because there are thinner, smaller, and because they undergo massive inelastic deformation. The toughness of this type of scale appears to be so high that it is not possible to fracture them using conventional fracture test configurations. In this paper we demonstrate that teleost fish scales from striped bass (*Morone saxatilis*) are notch insensitive, an indication of high toughness. Using a new miniaturized fracture test setup we then report, for the first time, the fracture toughness of teleost scales from striped bass (*M. saxatilis*) along different directions. The fracture toughness of the bony layer, collagen layer and non-collagenous interfaces were also measured. We finally use a set of simple fracture mechanics models to assess the main contributors of the high toughness of fish scales.

2. The hierarchical structure of scales from striped bass *Morone saxatilis*

Like many other biological materials (Fratzl and Weinkamer, 2007), fish scales display a hierarchical structure organized over several length scales (Fig. 1) (Zhu et al., 2012). Individual scales of striped bass are roughly pentagonal in shape and about 8–10 mm in diameter. Topological features on the surface of the scale, together with the underlying microstructure define different sectors on the scale: anterior (A), posterior (P) and lateral (L) regions. The anterior region of scales exhibits a triangular shape with radial grooves (radii) and circular rings (circuli) forming around the central area of the scales called "focus" (Zhu et al., 2012). While radii are only present in the anterior field, circuli also appear in the posterior region but their circular form is not well recognized (Zhu et al., 2012). It is believed that radii promote the flexibility of the scales and circuli are involved in the anchoring of the scale into the dermis (Zhu et al., 2012). Scales are the thickest at the focus region (300–400 μm), and the thickness decreases continuously towards the edges. A cross section of the scale reveals two distinct layers: the outer layer which is partially mineralized (hydroxyapatite volume fraction of 30% (Zhu et al., 2012)) and often called "bony layer", and the inner layer which undergoes less mineralization (hydroxyapatite volume fraction of 6%) and is referred to as "collagen layer" (Fig. 1). Each layer is composed of approximately 10–20 plies each ~5 μm thick, which are composed of fibrils of collagen type I. Plies "R" are composed of fibrils aligned along the radial direction while plies "C" are composed of fibrils

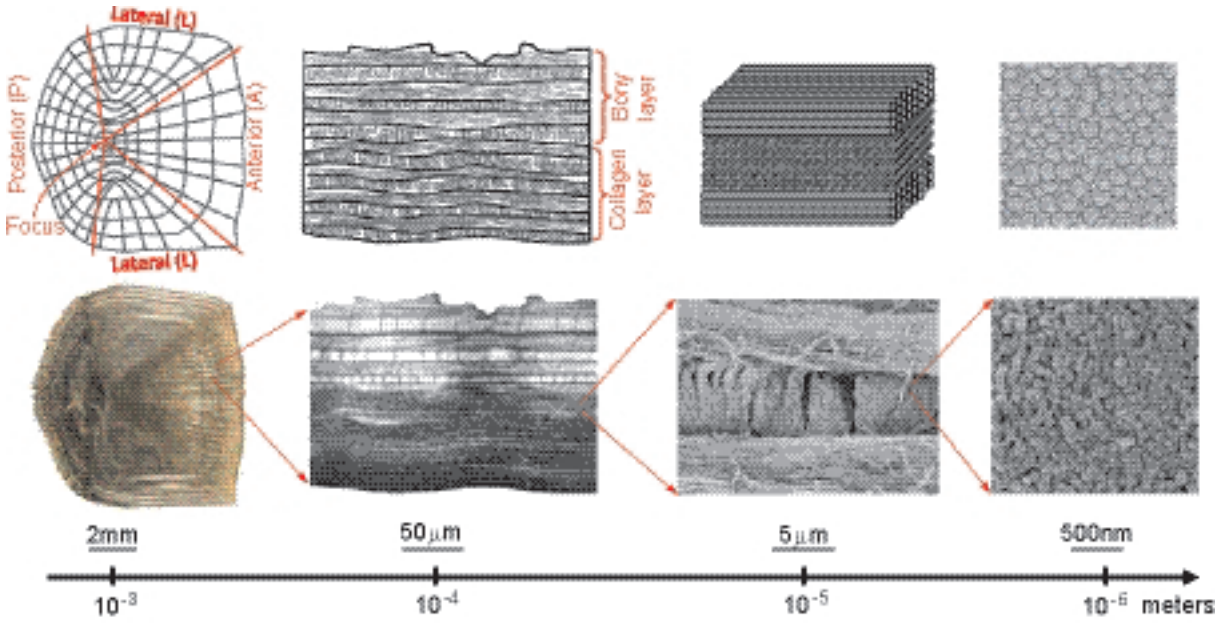

Fig. 1 – The hierarchical structure of individual fish scales, from mesoscale to nanoscale. (adapted from (Zhu et al., 2012)).

forming concentric pentagons centered on the focus of the scale. Plies "R" and "C" are alternatively stacked to form a multilayered structure. At the local scale, the collagen from the "R" and "C" layers cross at a right angle, locally forming a cross ply microstructure (Zhu et al., 2012). A compound of non-collagenous proteins hold the collagen fibrils together. These ingredients are found in virtually all collagen-based mineralized tissues such as bone, with the ratio of these components varying with the function of the tissue (Currey, 1999). Interestingly, unlike collagen in skin, tendon or ligaments, the collagen fibrils in fish scales are relatively straight and do not display the crimps which are often present in other soft collagenous tissues (Zhu et al., 2012).

3. Notch performance

The ability of the material to redistribute stresses around cracks or imperfections to eliminate stress concentration and delay fracture is critical to the robustness of both engineering and biological materials (Evans, 1997; Evans et al., 2001). High toughness and inelastic deformations are required for a redistribution of stresses to operate, and studies on engineering materials have shown that materials which can undergo tensile inelastic strain of at least four times the elastic strain completely suppress stress concentration notch insensitive (Davis et al., 2000). Fish scales are subjected to extreme loading which are concentrated over small surfaces and volumes in the case of a predator's attacks, and resisting high stress concentrations is critical to the performance of the scale and to the survival of the fish. Previous studies on the tensile response of fish scales from striped bass showed maximum elastic strains of about 5% and strain at failure of about 30%, accompanied with extensive inelastic deformations. These large deformations suggest that fish scales are notch insensitive, and in this section we actually tested this hypothesis. Fresh striped bass (*M. saxatilis*) was purchased from a fish supplier (Nature's Catch, Inc., Clarksdale, MS, USA), and scales were plucked using tweezers and stored in a freezer at −20 °C until testing. Prior to testing the scales were thawed in water at room temperature for 5 min. In order to assess the notch sensitivity of fish scales we prepared two batches of samples: the first batch consisted of tensile specimen prepared by cutting away two half-disks from the lateral regions of individual scales using a sharp multi-tube rotary hole-punch (5.6 mm diameter). This simple process produced a dog-bone shape tensile specimen with a gage width of about 4 mm (Fig. 2a). The second batch consisted of the same sample geometry, with the addition of a deep notch introduced with a razor blade about half-way across the width of the sample (Fig. 2b). The prepared intact and notched tensile specimens were then mounted on a miniature loading stage (Ernest F. Fullam Inc., Latham, NY) to be tested along the anterior–posterior direction. All the tests were performed in hydrated conditions, while a digital camera was used to record pictures during the course of the tests.

Fig. 2c shows typical force–displacement curves for intact and notched specimens. The curves have a bell shape, with an initial linear response followed by large tensile strains and tremendous energy absorption. As expected, the notched samples were weaker than the intact samples because of the presence of the notch and the associated reduction in the nominal cross section (i.e. minimum load bearing cross section). Based on this data, the nominal stress was computed by dividing the tensile force by the nominal cross section. The cross section used to compute the stresses in the intact sample was obtained by multiplying the width of the sample in the middle of the gage region (~4 mm) by the sample thickness (~300 μm). For the notched sample the nominal cross section is the width of the ligament after the notch was introduced (~2 mm) multiplied by the sample

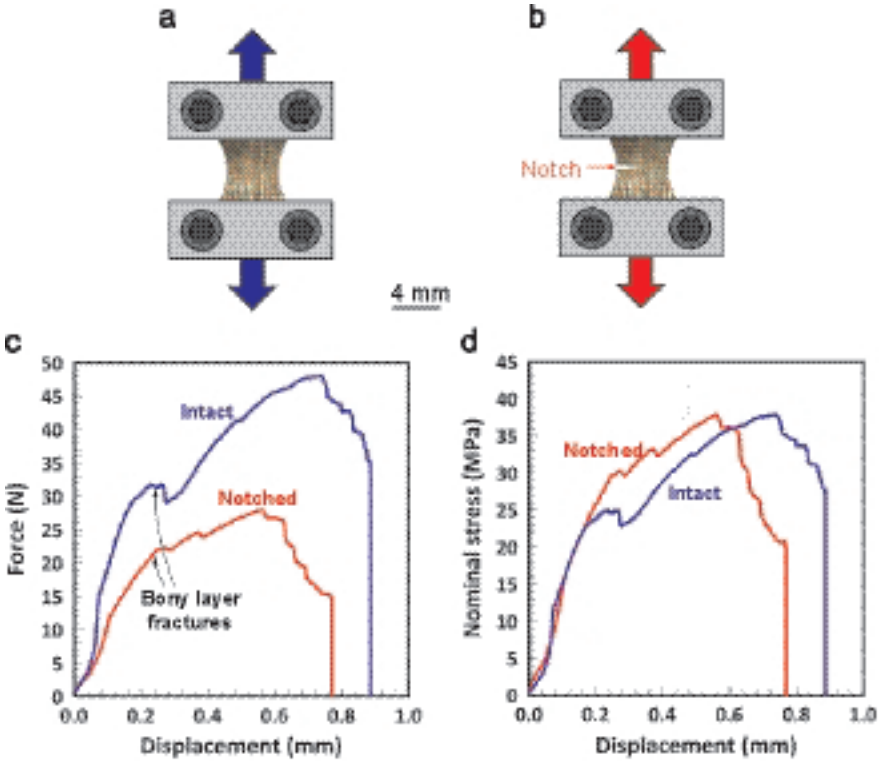

Fig. 2 – Schematic illustration of (a) intact tensile sample and (b) notched tensile sample; (c) typical force–displacement for intact and notched samples and (d) corresponding nominal stress–displacement curves.

thickness (~300 μm). The exact dimensions of the cross section were measured for each sample. Fig. 2d displays typical nominal stress–displacement curves obtained for intact and notched tensile specimens. Note that these experiments were intended to compare nominal stresses in notches and intact samples, and the exact strains in the sample were not computed (full tensile stress–strain curves for this type of fish scale can be found elsewhere (Zhu et al., 2012)). Remarkably the curves for the intact and notched samples are virtually identical. We found a nominal strength of 32.2±6.6 MPa for the intact samples and a nominal strength of 35.0±4.2 MPa for fracture samples ($N=5$ samples tested for each group). The failure modes in intact and notched samples were also identical: at the early stage of loading, the bony and collagen layer delaminated because of mismatch between their mechanical properties (Zhu et al., 2012) (Fig. 3b). Further increase of loading resulted in the fracture of bony layer while the collagen layer was still deforming, with extensive defibrillation of the collagen cross plies up to the ultimate failure at around 0.8 mm displacement. Because of variation in the thickness of the bony layer (bony layer is thicker at focus region), the fracture of bony layer in all the samples occurred at a region between the clamped site and notched area. Intact and notched samples also displayed stress whitening, an indication of delamination between bony and collagen layer occurs and also of region at which damage is accumulated (mainly in the bony layer). In bony and collagenous materials, whitening has also been associated in the past with inelastic deformation and with the formation of ligaments (Thurner et al., 2007). The notched sample also showed crack blunting (Fig. 3b and c), a potent toughening mechanism for metals and polymeric materials. Blunting was accompanied by a whitening of the material ahead of the notch and eventually across the entire ligament.

Finally the ligament ahead of the notch completely defibrillated and collapsed in tension, with no apparent crack propagation. This mechanism is similar to tendon, another high-performance material composed of unidirectional collagen fibrils (Ker, 2007). Fish scale are therefore notch insensitive: the stress concentration introduced by the notch is completely suppressed by micro-mechanisms associated with the cross-ply structure of the scale, and the only decrease in apparent strength is due to the reduction in nominal cross section. The toughening mechanisms are so powerful in fish scales that the pre-crack simply does not propagate, while the ligament undergoes massive non-linear deformations and yielding. Since the sample fails by collapse of the ligament instead of fracture, fracture toughness measurements are not possible from this configuration. We therefore developed another approach to force crack propagation through the scale, which we describe in the next section.

4. Fracture toughness of the whole scale

The experiments in the previous section showed that fish scales from striped bass are notch insensitive even in the presence of a deep notch half way across the scale. The samples failed by inelastic deformation and collapse rather than crack propagation. Therefore stress concentrations, generated for example by a sharp indenter, can be ignored

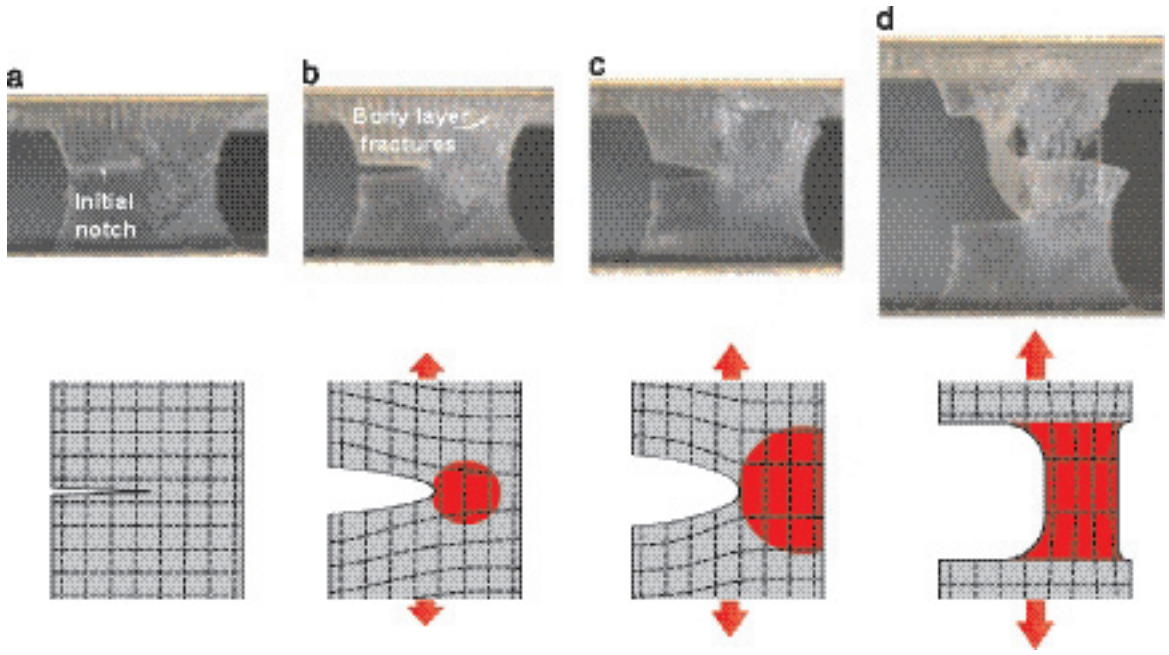

Fig. 3 – Sequence of images taken during the notch performance test with diagrams: (a) initial geometry of the notched sample; (b) bony layer fractures and delaminates; (c) crack blunting and propagation of inelastic region in collagen layer; (d) extensive defibrillation of the collagen layer and massive inelastic deformations in the collagen layer. There is no obvious crack propagation. The red region indicates inelastic deformation and processes.

in the scales and a criterion based on "strength" or "yielding" would be appropriate and sufficient to predict the failure of these scales. Nevertheless, it is useful to determine fracture toughness in the more general context of the fracture mechanics of collagenous tissue and of bio-inspiration. Notch insensitivity is an indication of high toughness, so in terms of designing notch insensitive materials it is useful to know what the toughness of the scales is. Toughness can also be correlated with structure and micromechanics to provide more insights into material design. The toughness of scales can also be compared with the toughness of existing collagenous tissues, with useful insights into structure–property relationships. In the natural fish scale we tested, the notch length and sample size is in the same order as the process zone. In a hypothetical larger fish scale, or a possible biomimetic fabric inspired from fish scales, the size of the notch and of the component can be much larger, and material nonlinearities may not be sufficient to suppress the effects of stress concentration at the crack tip (as seen in oxide fiber composites (Zok, 2006)). In these cases, failure may be governed by fracture mechanics rather than inelastic deformations and "yielding". Measurements of toughness on the fish scales from striped bass proved challenging. The scales are relatively compliant, small and extremely tough, and all the conventional fracture tests configurations we tried were unsuccessful in propagating cracks and in producing meaningful measures of toughness. Compact tension fracture tests (with pre-notch and forces transmitted though pins) resulted in large out-of-plane warping of the samples. In bending configurations, the sample underwent large deflections without any crack propagation. In order to overcome these limitations we used a pair of miniature custom made miniature fixtures made of stainless steel in order to clamp the scales (Fig. 4). This configuration promotes crack propagation and limits in-plane and out-of-plane deformations. Slippage at the clamp is also limited, because large surfaces of the scale are used for clamping. The test geometry is similar to the rigid double cantilever beam (RDCB) fracture test, which we recently developed to measure the fracture toughness of biological proteins and engineering adhesives (Dastjerdi et al., 2012). Here the fracture samples were prepared by punching six holes (1 mm in diameter) though the scale: two pairs of holes were used as screw holes to clamp the scale with the two pairs of rigid steel fixtures, while the other pair was used as pin holes to exert opening forces with the miniature loading machine (Fig. 4a and c). In order to monitor the crack propagation process, a gap of ~1 mm was kept between the two clamps, so the sample configuration consisted of a rectangular strip of fish scale clamped to two rigid plates. After clamping the scale, a deep cut about 3 mm long was introduced on the side of the scale with a fresh razor blade. The clamped samples were finally placed in a miniature loading stage mounted with two pins, and installed under an upright, reflected light microscope (BX-51M, Olympus, Markham, Canada) equipped with a CCD camera (RETIGA 2000R, Qimaging, Surrey, Canada) to monitor crack propagation. All tests were performed at an opening displacement rate of 5 $\mu m\ s^{-1}$ and in a fully hydrated condition (the gap between the fixtures was filled with water). In order to investigate possible anisotropy in toughness, cracks were propagated along three different directions: anterior–posterior (A–P), lateral–lateral (L–L) and posterior–anterior (P–A) (Fig. 4b).

Crack propagation was very stable, an indication of powerful toughening mechanism within the scale. The force–

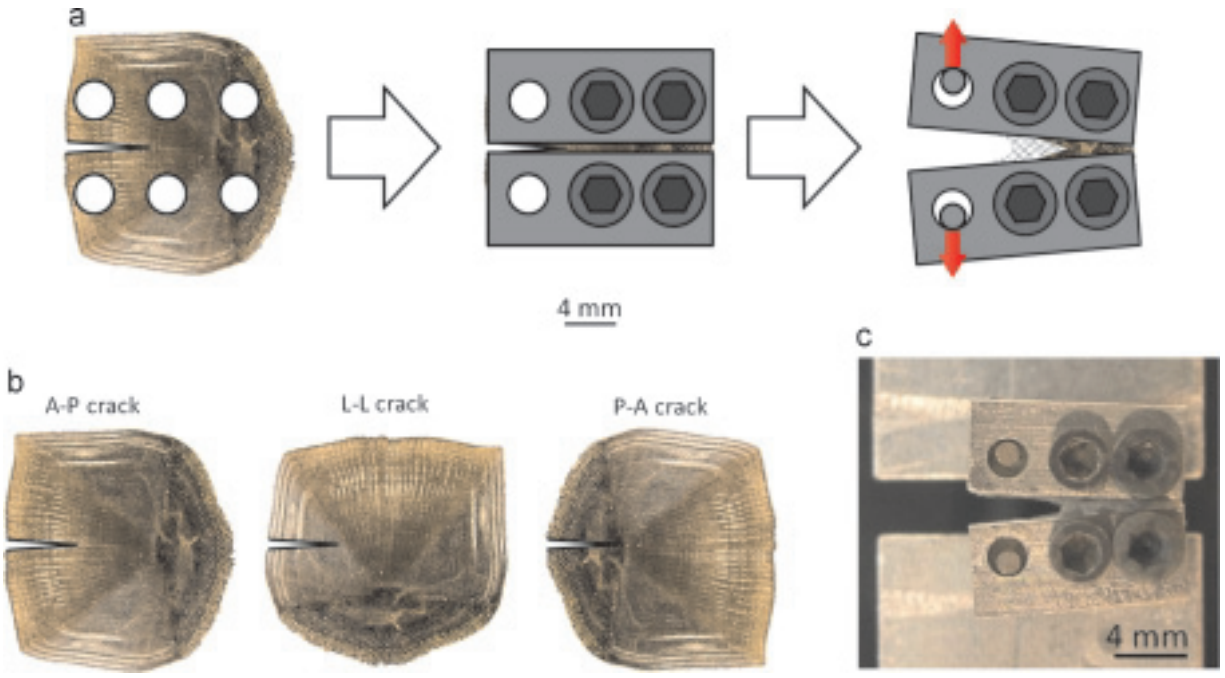

Fig. 4 – (a) Preparation and testing of the fracture sample; (b) the three orientations explored for crack propagation; (c) actual picture of an ongoing fracture test.

displacement curves (Fig. 5a) also displayed a bell shape, a characteristic of tough materials. All curves showed an initial quasi-linear region with a stiffness of 15–20 N mm^{-1}, followed by softening as damage accumulated and the crack propagated in the fish scale. Damage accumulation continued until a maximum load, after which the load progressively decreased. Examinations of in-situ optical images revealed that the sudden drop of force after the point of maximum load corresponds to the brittle fracture of the bony layer. Fig. 5b shows an optical image captured just after the peak load for A–P crack propagation, showing an entirely fractured bony layer. At this point the underlying collagen has undergone massive defibrillation, but intact fibrils are still bridging the opening crack. The water saturating the crack made imaging difficult, but defibrillated collagen at 30–60° from the crack faces could be observed behind the crack tip (Fig. 5c). Fig. 5d shows a schematic of the structure of these fibrils. The fibers belonging to the circumferential layer "C" crossed the propagating crack at 90°. These fibers were pulled out from the collagen layer, and probably failed at moderate crack openings. Another type of fibers from the radial "R" layer delaminated from the collagen layer as the crack propagated, continuously feeding collagen fibrils into the opening crack. We observed more of these fibers than the "C" fibers, probably because the fibers from the "R" layer could bridge the crack over greater crack opening distances. In summary, once the brittle bony layer has fractured, simultaneous crack bridging of fibers from the "R" and "C" layer appears to be the main cohesive mechanism in fish scales. Crack bridging is a powerful toughening mechanism which was observed in other natural composites including bone (Nalla et al., 2003), nacre (Zhu et al., 2013), and tooth enamel (Imbeni et al., 2005).

Here we determined the fracture toughness of the scales using the "work of fracture" which is the energy (area under force–displacement curve) required to fracture the notched specimen divided by the area of the fractured surface. Work of fracture can also be interpreted as the average energy per unit thickness required to propagate the crack by a unit distance, and in that sense it directly correlates with the energy definition of fracture toughness based on J-integral. Fig. 5b shows the work of fracture obtained for the three different directions of crack propagation: anterior–posterior (A–P), lateral–lateral (L–L), and posterior–anterior (P–A). We found a toughness of 17.6 ± 0.5 kJ m^{-2}, 15.3 ± 1.1 kJ m^{-2}, and 18.4 ± 0.7 kJ m^{-2} for A–P, L–L, and P–A directions, respectively, which are remarkably high values compared to bone (1–10 kJ m^{-2}) (Koester et al., 2008) or even mammalian skin (10–20 kJ m^{-2}) (Purslow, 1983). The fracture toughness appears to be slightly lower in the L–L direction, and further statistical analysis (Student's *t*-test) confirmed that the work of fracture along the L–L direction is statistically significantly lower ($p < 0.05$) than in the A–P and P–A direction, which were statistically the same. A slightly lower toughness in the L–L direction can promote crack propagation across the scale, which may ultimately result in "clipping" of the scale and minimal consequences for the animal. In contrast, cracks propagating towards the anterior region of the scales may be more dangerous, because they can provide pathways to bacteria and other external agents towards the softer underlying tissues. We conclude this section by a few remarks on the failure model and measurement of work of fracture. Since the scale is notch insensitive for this specimen size and notch length, the failure was dominated by inelastic collapse. A sample with a shorter notch or even no notch would produce the same work of fracture. In either of these cases, a mode I tearing of the scale is imposed by the progressive opening of the stiff clamps. In practice, testing specimens with shorter notches was not possible because the samples slipped out of

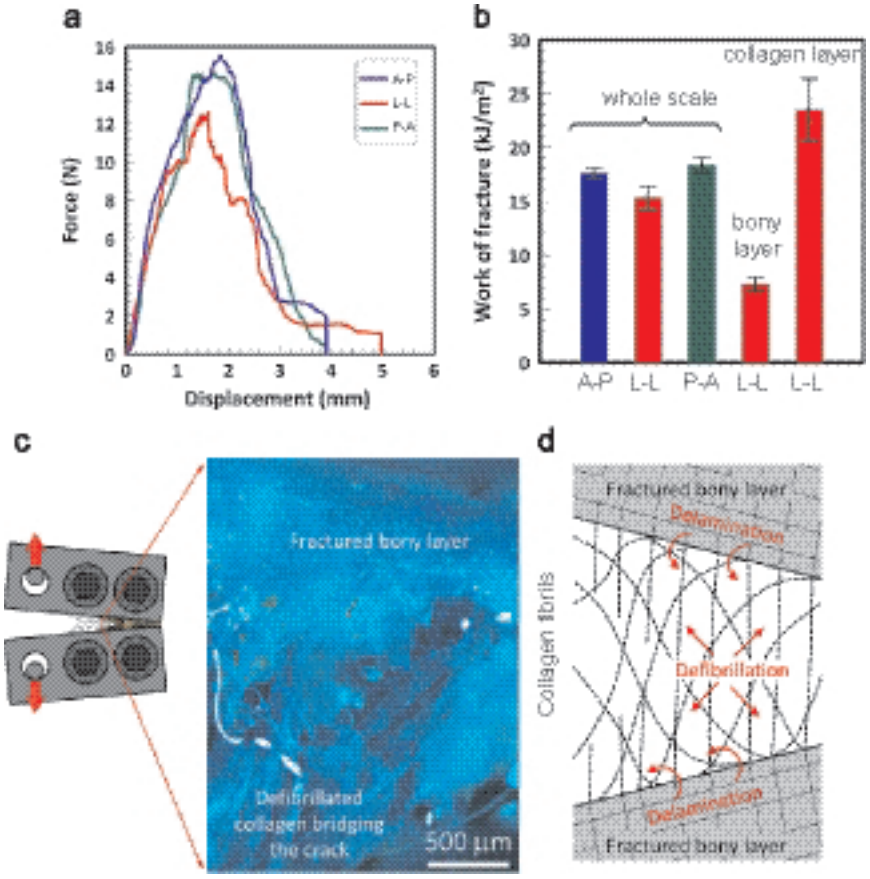

Fig. 5 – (a) Typical force–displacement curves obtained from fracture experiment for the three directions of crack propagation: (b) corresponding work of fracture; (c) optical image taken during the softening region of the force–displacement curve (A–P crack propagation) showing the fractured bony layer and extensive defibrillation of the collagen layer; (d) schematic showing the structure of the defibrillated collagen during the course of crack opening.

the grips before crack propagation started. During the test, we also could not observe and locate a crack tip in the traditional sense, because of blunting, defibrillation and massive inelastic deformations. It is in fact likely that the inelastic region spreads across the entire scale ahead of the notch before or shortly after crack propagation occurs. Nevertheless, the results from the experimental setup used here directly reflect the traction–separation behavior of the material, and we have indeed recently used a similar setup to determine cohesive laws of various adhesive in the past, with modeling and validation against independent toughness measurements (Dastjerdi et al., 2012, 2013). In this experimental configuration, the energy dissipated up to failure can therefore be used to compute work of fracture and toughness, even if the inelastic region extends along the entire sample.

5. Fracture toughness of bony and collagen layers

Crack propagation across the scale involves fracturing both bony and collagenous layers, two materials with distinct compositions and high contrast of properties. In the context of developing biomimetic systems inspired from scales, it is important to determine the individual properties for the bony and collagenous layers. In this section we measured the fracture toughness of each of the individual layers, using direct measurements and indirect methods. Following protocols developed in previous work on fish scales (Zhu et al., 2012), the collagen layer was carefully ablated from a scale. The remaining material, made entirely of bony material, was more brittle than the collagen layer, so that traditional fracture toughness tests could be used. The bony layer was cut into a dog-bone shape (with gage width and length of 2 mm) using a laser engraver (Mirkhalaf et al., 2014) with its longitudinal direction parallel to the A–P axis. A 1.5 mm long pre-notch was then introduced across the gage region using laser engraving. During the whole process of cutting, the scales were kept hydrated in order to cool the sample and to avoid shrinkage of the samples from drying. The samples were then tested in tension using the miniature loading stage and hydrated conditions. The samples showed much less deformations compared to the whole scale, but fracture propagation was still stable. We found a work of fracture of $J_B = 7.3 \pm 0.7$ kJ m^{-2} for the bony layer, which is about two times lower than the work of fracture for the whole scale. Meanwhile, none of the samples of pure collagen obtained from the ablation protocol could be tested for fracture toughness as they would invariably slip out of the grips. The toughness of the collagen layer could however be

estimated from the toughness of the whole scale and of the bony layer. Propagating a crack through the whole scales involves the fracture of both bony and collagen layers. Since these two layers have approximately the same thickness, the fracture toughness of the whole scale J_S can be estimated by:

$$J_S \approx \frac{1}{2}(J_C + J_B) \quad (1)$$

where J_C and J_B denote the fracture toughness of the collagen and bony layer, respectively. Eq. (1) does not take in account the interactions between bony and collagen layers (which probably exist), but provides a means to evaluate the toughness of the collagen layer which we could not obtain experimentally. J_S and J_B are known from the experiments described above, and Eq. (1) yielded a fracture toughness of $J_C = 23.5 \pm 2.9\ \mathrm{kJ\,m^{-2}}$ for the collagen layer, which is more than three times the toughness of the bony layer. While both bony and collagen layers are composed of collagen fibrils with almost the same arrangement, it is probably the higher concentration of brittle hydroxyapatite within the bony layer which results in its lower fracture toughness compared to the collagen layer.

6. Interlaminar fracture toughness within individual scales

Collagen is a high-performance fiber, and its high deformability and high strength generate, for a large part, the toughness of fish scales. Equally important is the cohesion between the collagen fibrils. As observed above pullout, delamination and defibrillation play an important role in the toughening mechanisms operating in the scale, and these mechanisms are governed by the toughness of the extracollagenous proteins at the boundaries between the fibrils. In order to determine the interlaminar fracture toughness of individual scales, we performed a series of peel tests in hydrated condition. For this test, the scales were cut into rectangular strips of 8×4 mm, with their length parallel to the A–P axis of the scales (Fig. 6a).

In order to facilitate handling and testing, the scale was demineralized in Surgipath Decalcifier II (Leica Microsystems Inc., Buffalo Grove, IL) following standard procedures. Using a fresh razor blade the scale was partially delaminated in order to introduce a pre-notch about 4 mm deep. The ends of the sample were then clamped in the miniature loading stage as shown in Fig. 6b. The samples were then loaded at a rate of $5\ \mu\mathrm{m\,s^{-1}}$ until the material was completely debonded. The samples were kept hydrated throughout the tests by frequent irrigation with water. The propagation of the interlaminar crack was very stable until the end of the test where the collagen and bony layer completely separated, and post-mortem imaging revealed that the crack tended to follow the interface between bony and collagen layer. Fig. 6c shows two typical force–displacement curves from this test. Following elastic loading, delamination of the scale commenced at a constant force of about 0.05 N. At a displacement of about 5 mm (corresponding to a crack propagation of 2.5 mm), the force increased continuously up to about 0.12 N at which the strip completely delaminated. The ultimate force was reached at a displacement of 8 mm, corresponding to a crack advance of 4 mm (which was the length of the remaining material after the initial notch was produced. The increase of force from 5 to 8 mm (corresponding to the anterior and focus field of individual scales) indicates that the interlaminar strength of collagen layers most likely increases from anterior to focus area. The toughness of the interface, in energy terms, was simply obtained by dividing the area under the force–displacement curves by the area of the fractured surface. This calculation yielded a toughness of $38.6 \pm 9.8\ \mathrm{J\,m^{-2}}$. For comparison this delamination toughness is about twenty times higher than office tape on a glass substrate (Dastjerdi et al., 2012), and more than ten times higher than the toughness of the interfaces in nacre (Dastjerdi et al., 2013). The delamination toughness is 400 times lower than the toughness of the whole scale measured above which is beneficial, considering that low interfacial toughness is a requirement for pullout, delamination and defibrillation of the collagen in the fracture process of the whole scale in the A–P, L–L and P–A directions.

7. The fracture mechanics of fish scales

The previous sections demonstrated the high toughness of fish scales from striped bass, suggesting that this material could serve as model for bio-inspired protective materials and systems. However, in order to establish design principles

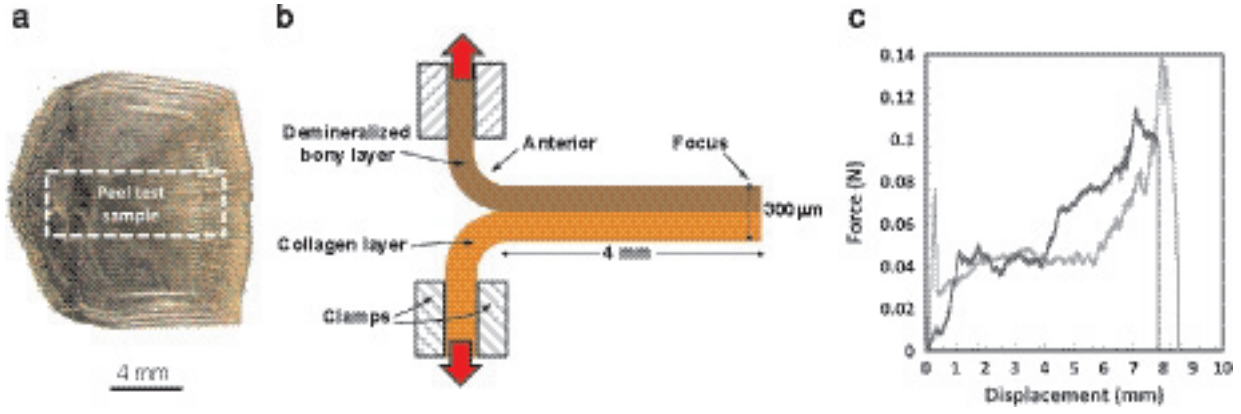

Fig. 6 – (a) Picture showing the peel test sample geometry and orientation; (b) schematic illustration of peel test setup for measuring the delamination toughness of individual scales; (c) two typical force–displacement curves obtained from this test.

for such material, a deeper understanding of the fracture mechanics of fish scales is required. In this section we present models which capture the crack resistance produced by collagen fibrils. The first model examines the contribution of process zone toughening, where the energy dissipated in a strip of material around the crack generates fracture toughness. In a second section we examine the potential contribution of fiber delamination on crack bridging. The models focus on the fracture mechanics of the tougher collagen layer. Similar mechanisms may operate in the bony layer but to a lower extent, because the mineralization of the fibrils limits their extension.

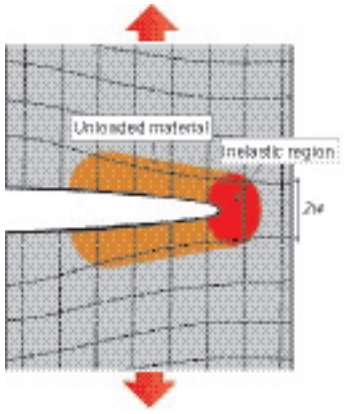

Fig. 7 – Process zone toughening in the collagenous layer of the fish scale in a steady state configuration. The frontal zone (size 2*w*) leaves a wake of inelastically deformed material behind the crack tip.

7.1. Process zone toughening

Experimental observations showed that massive nonlinear deformations ahead of the crack and in its wake are a prominent feature in the process of fracturing the scale. Fig. 7 schematically shows a crack propagating through the collagenous layer, where the material "yields" just ahead of the crack tip because of high stresses. Once the crack propagates through the initial inelastic region the materials near the crack face unloads, and the process of loading/unloading dissipates energy (Shen et al., 2008). Assuming that the yielding is governed by tensile stress only, the half width of the yielded region is given by Evans et al. (1986), Barthelat and Rabiei (2011):

$$w = 0.25\frac{J_C E_C}{{\sigma_C}^2} \tag{2}$$

where σ_C is the yield strength of the collagen layer in tension, J_C is the toughness of the collagen layer and E_C is its elastic modulus. Using the experimental values $J_C \approx 23\ \mathrm{kJ\ m^{-2}}$, $E_C \approx 0.5$ GPa and $\sigma_C \approx 60$ MPa Eq. (2) gives $w \approx 0.8$ mm, which is consistent with experimental observations. Since the spacing between the clamps was also in the order of millimeters, it is possible that the inelastic region was constrained by the clamps. Unfortunately it was not possible to increase the spacing between the clamps; these attempts resulted in the reduction of the clamping area and in the sample slipping out of the grips. Constraining this region may have therefore resulted in underestimating the actual toughness of the scale, an effect similar to cracks propagating in ductile adhesives (Tvergaard and Hutchinson, 1996).

The toughness contribution of the energy dissipated upon loading (ahead of tip) and unloading (behind the tip) is given by Evans et al. (1986), Barthelat and Rabiei (2011), Gao (2006):

$$J_P = 2wU_C \tag{3}$$

where U_C is the density of energy absorbed by the collagen layer in tension, and w is the half of the width of the inelastic region. From previous experimental tensile stress–strain data we measured $U_C \approx 12\ \mathrm{MJ\ m^{-3}}$. With this value Eq. (3) predicts $J_P \approx 19\ \mathrm{kJ\ m^{-2}}$, which is close to the experimental toughness ($J_C \approx 23\ \mathrm{kJ\ m^{-2}}$). The model therefore suggests that the massive inelastic deformations ahead and behind cracks in fish scales are the primary source of their toughness.

7.2. Delamination bridging in the R layer

Another prominent feature observed in the fracture experiments is the delamination of the collagen fibers within the opening crack. These delaminated fibers have the potential to generate closure forces and to bridge the crack walls, in a manner similar to laminated composites (Sorensen et al., 2008) and cortical bone (Nalla et al., 2004). Fig. 8a shows a crack propagating through the radial layer. Experimental observations suggest that a crack propagating along the radial fibers generate massive delamination of bundles of fibrils from the crack faces. As the crack opens the delaminated fibrils stretch, generating closure forces on the crack faces. Because of the very high aspect ratio of the fibers, we neglect the energy stored by shear and bending deformations and we focus on tensile deformation. Fig. 8b shows an individual fiber (i.e. a bundle of fibrils) which was delaminated from the crack faces. As the crack opens, the fiber stretches and also continues to delaminate from the crack faces. Fig. 8c shows the same fiber with the tensile force F exposed. The fiber has modulus E_f, and to keep the model simple we assume that the fiber has a square cross section with dimension $d \times d$. The toughness of the interface (in energy terms) between fibers is noted J_i. The mechanics of this system is in many ways similar to the peel test, examined by Kendall (Kendall, 1975) in the steady state delamination crack propagation regime. By balancing the elastic energy released by the fiber with the toughness of the interface (in energy terms) the Kendall model gives:

$$J_i = \frac{1}{2}\left(\frac{F}{d}\right)^2 \frac{1}{E_f d} + \frac{F}{d}(1 - \cos\theta) \tag{4}$$

In our case the extension of the fiber and the delamination length are coupled, so the stretch of the fiber can be written as:

$$\varepsilon = \frac{l}{l_0} - 1 \tag{5}$$

The force F carried by the fiber can then be written using Hooke's law and some trigonometry in Fig. 8c:

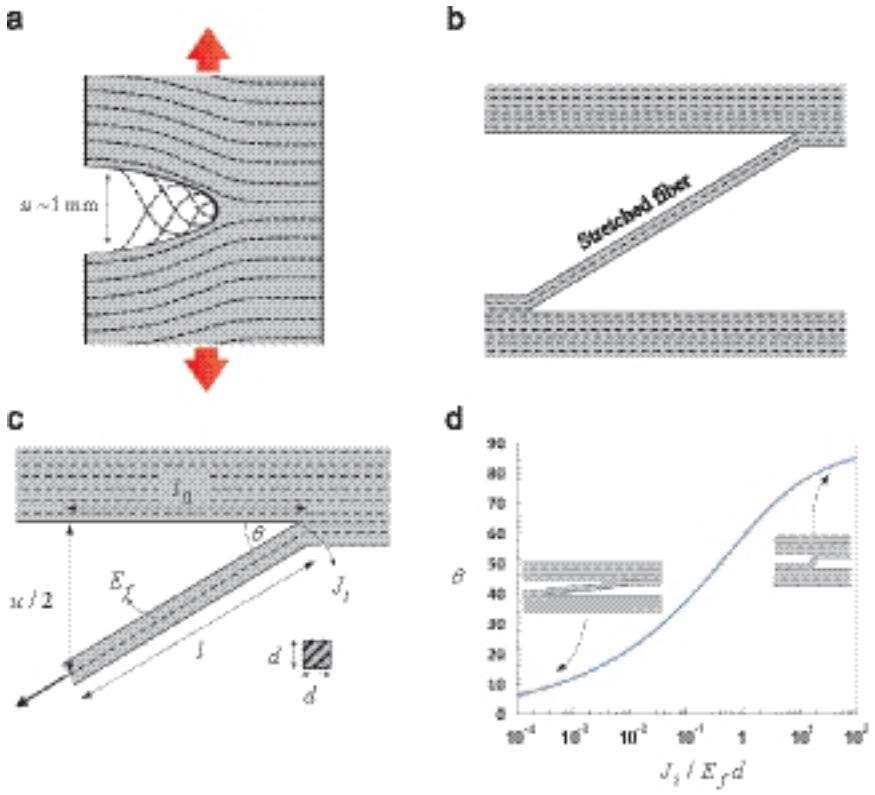

Fig. 8 – (a) Schematic of a crack propagating along the radial layer (b) fibers delaminated from the crack faces bridge the crack; (c) diagram used to develop the mechanical model; (d) delaminated fiber angle as a function of nondimensional parameter $J_i/E_f d$

$$F = d^2\sigma_f = E_f d^2\left(\frac{1}{\cos\,\theta} - 1\right) \tag{6}$$

where σ_f is the tensile stress in the fiber. Eqs. (4) and (6) can now be combined, leading to:

$$\frac{J_i}{E_f d} = \frac{1}{2\cos^2\theta} + \cos\,\theta - \frac{3}{2} \tag{7}$$

This result implies that in the steady state the angle of the delaminated fiber θ is not a function of crack opening. The angle depends only on the properties and geometry of the fiber (E_f and d) and on the toughness of the interface (J_i). Fig. 8d illustrate the predictions of Eq. (7). Stiff fibers and weak interfaces (low $J_i/E_f d$) lead to long delamination distance but small delamination angle, with little deformation in the fiber. In contrast, soft fibers bonded by tough interfaces (high $J_i/E_f d$) lead to shorter delamination distance but high delamination angle, accompanied with high strain in the fiber. We now use the properties of the collagen fibers and of their interfaces in the model. Using $E_f \approx 1$ GPa (Shen et al., 2008), $d \approx 1$ μm from optical imaging and $J_i \approx 40\,\mathrm{J\,m^{-2}}$ as measured above gives $J_i/Ed \approx 0.04$. With this value the model predicts a fiber angle of about 30° within the delaminated region, which is consistent with experimental observations (Fig. 5c). With this angle, Eq. (6) predicts a tensile force $F \approx 150$ μN per fiber, corresponding to a stress of $\sigma \approx 150$ MPa and a strain $\varepsilon \approx 0.15$. Independent experiments on collagen fibrils confirm that collagen fibrils can undergo such stress and strain without failing (Shen et al., 2008). We now turn our attention to the closure stress generated by the delaminated fibers. If the intact fibers are oriented at a small angle $\phi \ll \theta$ from the crack line, the density of fibers crossing the crack face is:

$$N_f = \frac{\sin\,\phi}{d^2} \tag{8}$$

The closure traction that the fibers exert on the crack faces is:

$$\sigma_b = N_f F\,\sin\,\theta \tag{9}$$

Combining Eqs. (6), (8) and (9) gives:

$$\sigma_b = E_f\,\sin\,\phi\left(\frac{1}{\cos\,\theta} - 1\right)\sin\,\theta \tag{10}$$

Finally the effect of the closure stress on toughness can be approximated with:

$$J_b \approx \sigma_b u \tag{11}$$

where u is the crack opening at which the bridging stress vanishes. Using $E_f = 1$ GPa, $\phi \approx 5°$ and $\theta = 30°$ gives a closure stress of $\sigma_b = 6$ MPa. The model therefore suggests that while experimental observations show massive delamination of the fibers, the closure stress exerted by the delaminated fibers account for a small portion of the tensile strength of fish scales. Using a crack opening $u \approx 1$ mm, Eq. (11) gives $J_b \approx 6\,\mathrm{kJ\,m^{-2}}$. Because delamination can exert closure stress over large crack openings and long bridging regions, the contribution of delamination on toughness is non-negligible, but remains smaller than the process zone toughening described above. These models are highly idealized, and in reality process zone and delamination and toughening are

probably highly coupled microscale phenomena. Nevertheless, the models provide useful insights into the main mechanisms behind the high toughness of fish scales.

8. Summary

Teleost fish scales are 500 million year old collagen-based materials constructed to provide flexible armored protection. To fulfill this function fish scales are extremely tough, a highly desirable properties which also makes fracture testing difficult. In this work we have shown that individual fish scales from *M. saxatilis* are indeed notch insensitive. Using a new miniature setup we measured the toughness of the scales along three crack propagation orientations in the whole scales, and proceeded to measuring the toughness of the individual bony and collagen layer which compose the scale. Our results show that these materials are amongst the toughest biological materials (in energy terms) for which fracture toughness data is available (Fig. 9). For comparison we also plotted the toughness of scales from alligator gar. For this type of ganoid scale the modulus is about 10 GPa and the toughness ranges from about 0.8 to 3.6 kJ m^{-2} (calculated using $J_{IC}=K_{IC}^2/E$), depending on the orientation of crack propagation (Yang et al., 2013a,b). Compared to these ganoid scales teleost scales are more compliant because of their lesser degree of mineralization but they are as tough in term of stress intensity (K_C), and one order of magnitude tougher in term of energy (J_C). The non-collagenous interfaces which hold the collagen fibrils together have a much lower (about 400 times) toughness. As a result the fibers can detach relatively easily, which explains the massive delamination and defibrillation observed in the experiments. Our fracture models suggest that inelastic deformations of the collagen fibrils, which operate over regions in the order of 1–2 mm around the crack tip is the main contributor to toughness, a process similar to nacre (Barthelat and Rabiei, 2011) and advanced engineering polymers (Evans et al., 1986). Delamination of the collagen fibers produce a small bridging stress across the crack faces, but this mechanism can operate over

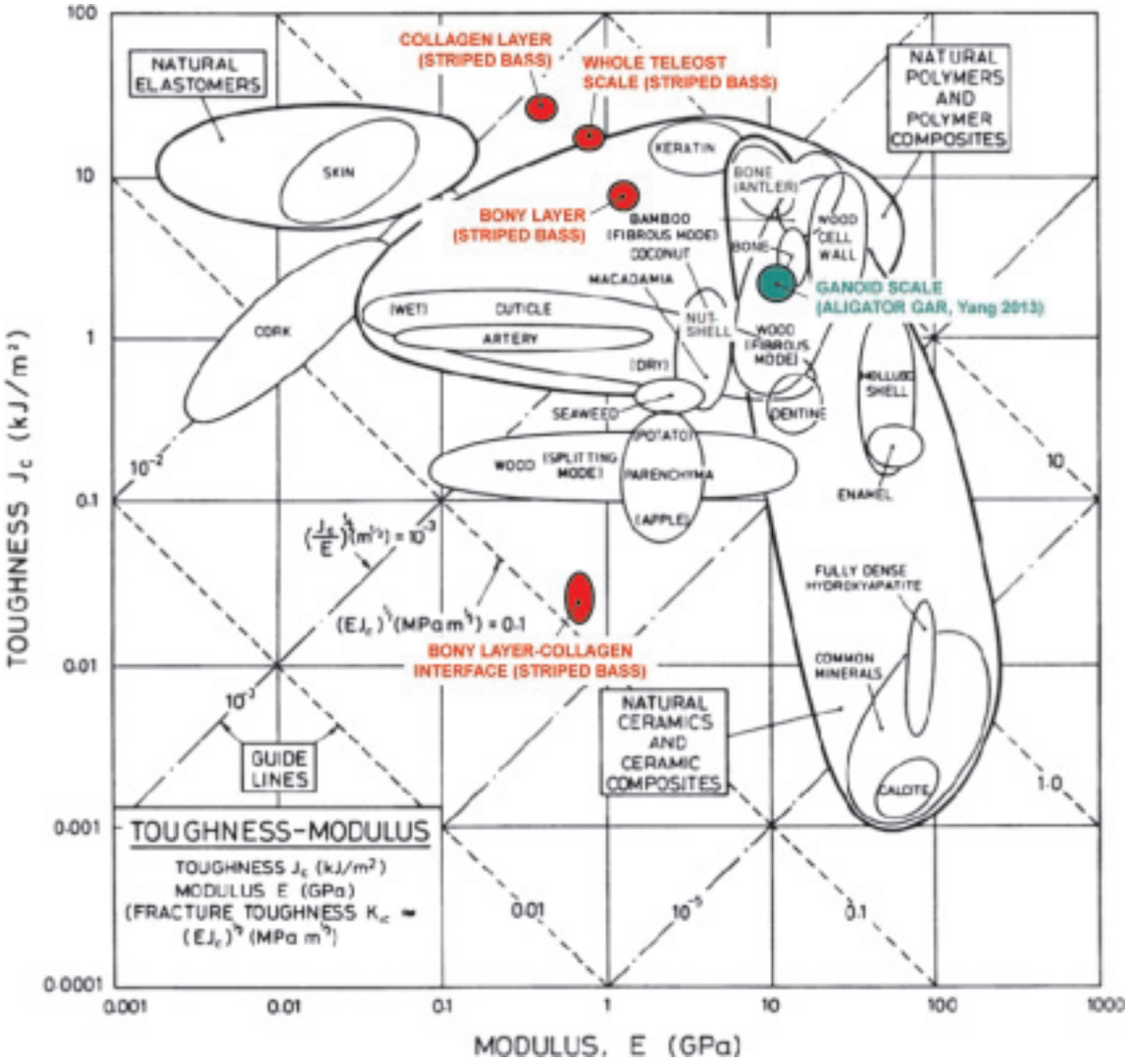

Fig. 9 – Toughness-modulus Ashby chart for natural materials. The properties of mechanical properties for whole teleost fish scales, bony layer, collagen layer and their interface are shown (adapted from (Wegst and Ashby, 2004)).

large crack openings and we found that its contribution to toughness is not negligible. These findings may suggest new strategies for light weight protective materials and fabrics which combine compliance, toughness and resistance to puncture and lacerations. More fundamentally, the properties and mechanisms of teleost fish scales provide useful hints on the behavior of similar collagenous tissues such as lamellar bone, tendon and ligaments.

Acknowledgement

This research was sponsored by a Discovery Grant from the Natural Sciences and Engineering Research Council of Canada. A.K.D was partially supported by a McGill Engineering Doctoral Award (MEDA).

REFERENCES

ASTM 2003, ASTM D1938–08: Standard Test Method for Tear-Propagation Resistance (Trouser Tear) of Plastic Film and Thin Sheeting by a Single-Tear Method.

Barthelat, F., 2007. Biomimetics for next generation materials. Philos. Trans. R. Soc. London, Ser. A 365, 2907–2919.

Barthelat, F., Rabiei, R., 2011. Toughness amplification in natural composites. J. Mech. Phys. Solids 59 (4), 829–840.

Benton, M.J., 2004. Vertebrate Paleontology, third ed. Blackwell Science Ltd..

Bonderer, L.J., Studart, A.R., Gauckler, L.J., 2008. Bioinspired design and assembly of platelet reinforced polymer films. Science 319 (5866), 1069–1073.

Browning, A., Ortiz, C., Boyce, M.C., 2013. Mechanics of composite elasmoid fish scale assemblies and their bioinspired analogues. J. Mech. Behav. Biomed. Mater. 19, 75–86.

Bruet, B.J.F., et al., 2008. Materials design principles of ancient fish armour. Nat. Mater. 7 (9), 748–756.

Chintapalli, R., et al., 2014. Fabrication, testing and modeling of a new flexible armor inspired from natural fish scales and osteoderms. Bioinspiration Biomimetics, 9.

Currey, J.D., 1999. The design of mineralised hard tissues for their mechanical functions. J. Exp. Biol. 202 (23), 3285–3294.

Currey, J.D., 1999. The design of mineralised hard tissues for their mechanical functions. J. Exp. Biol. 202 (23), 3285.

Dastjerdi, A.K., et al., 2012. Cohesive behavior of soft biological adhesives: experiments and modeling. Acta Biomater. 8 (9), 3349–3359.

Dastjerdi, A.K., Rabiei, R., Barthelat, F., 2013. The weak interfaces within tough natural composites: experiments on three types of nacre. J. Mech. Behav. Biomed. Mater. 19, 50–60.

Dastjerdi, A.K., Tan, E., Barthelat, F., 2013. Direct measurement of the Cohesive Law of adhesives using a rigid double cantilever beam technique. Exp. Mech. 53 (9), 1763–1772.

Davis, J.B., Marshall, D.B., Morgan, P.E.D., 2000. Monazite-containing oxide/oxide composites. J. Eur. Ceram. Soc. 20 (5), 583–587.

Dimas, L.S., Buehler, M.J., 2012. Influence of geometry on mechanical properties of bio-inspired silica-based hierarchical materials. Bioinspiration Biomimetics 7 (3).

Evans, A.G., 1997. Design and life prediction issues for high-temperature engineering ceramics and their composites. Acta Mater. 45 (1), 23–40.

Evans, A.G., et al., 1986. Mechanisms of toughening in rubber toughened polymers. Acta Metall. 34 (1), 79–87.

Evans, A.G., et al., 2001. Model for the robust mechanical behavior of nacre. J. Mater. Res. 16 (9), 2475–2484.

Fratzl, P., Weinkamer, R., 2007. Nature's hierarchical materials. Prog. Mater Sci. 52 (8), 1263–1334.

Gao, H.J., 2006. Application of fracture mechanics concepts to hierarchical biomechanics of bone and bone-like materials. Int. J. Fract. 138 (1-4), 101–137.

Garrano, A.M.C., et al., 2012. On the mechanical behavior of scales from *Cyprinus carpio*. J. Mech. Behav. Biomed. Mater. 7, 17–29.

Ikoma, T., et al., 2003. Microstructure, mechanical, and biomimetic properties of fish scales from Pagrus major. J. Struct. Biol. 142 (3), 327–333.

Imbeni, V., et al., 2005. The dentin–enamel junction and the fracture of human teeth. Nat. Mater. 4 (3), 229–232.

Kardong, K.V., 2006. Vertebrates: Comparative Anatomy, Function, Evolution. McGraw-Hill, Boston.

Kendall, K., 1975. Thin-film peeling—elastic term. J. Phys. D: Appl. Phys. 8 (13), 1449–1452.

Ker, R.F., 2007. Mechanics of tendon, from an engineering perspective. Int. J. Fatigue 29 (6), 1001–1009.

Koester, K.J., Ager, J.W., Ritchie, R.O., 2008. The true toughness of human cortical bone measured with realistically short cracks. Nat. Mater. 7 (8), 672–677.

Lin, Y.S., et al., 2011. Mechanical properties and the laminate structure of Arapaima gigas scales. J. Mech. Behav. Biomed. Mater. 4 (7), 1145–1156.

Mayer, G., 2005. Rigid biological systems as models for synthetic composites. Science 310 (5751), 1144–1147.

Meyers, M.A., et al., 2008. Biological materials: structure and mechanical properties. Prog. Mater Sci. 53, 1–206.

Meyers, M.A., et al., 2012. Battle in the Amazon: Arapaima versus Piranha. Adv. Eng. Mater. 14 (5), B279–B288.

Mirkhalaf, M., Dastjerdi, A.K., Barthelat, F., 2014. Overcoming the brittleness of glass through bio-inspiration and micro-architecture. Nat. Commun., 5.

Nalla, R.K., Kinney, J.H., Ritchie, R.O., 2003. Mechanistic fracture criteria for the failure of human cortical bone. Nat. Mater. 2 (3), 164–168.

Nalla, R.K., Kruzic, J.J., Ritchie, R.O., 2004. On the origin of the toughness of mineralized tissue: microcracking or crack bridging?. Bone 34 (5), 790–798.

Purslow, P.P., 1983. Measurement of the fracture toughness of extensible connective tissues. J. Mater. Sci. 18 (12), 3591–3598.

Shen, Z.L., et al., 2008. Stress–strain experiments on individual collagen fibrils. Biophys. J. 95 (8), 3956–3963.

Sorensen, L., et al., 2008. Bridging tractions in mode I delamination: measurements and simulations. Compos. Sci. Technol. 68 (12), 2350–2358.

Studart, A.R., 2012. Towards high-performance bioinspired composites. Adv. Mater. 24 (37), 5024–5044.

Thurner, P.J., et al., 2007. High-speed photography of compressed human trabecular bone correlates whitening to microscopic damage. Eng. Fract. Mech. 74 (12), 1928–1941.

Tvergaard, V., Hutchinson, J.W., 1996. On the toughness of ductile adhesive joints. J. Mech. Phys. Solids 44 (5), 789–800.

Vernerey, F.J., Barthelat, F., 2010. On the mechanics of fishscale structures. Int. J. Solids Struct. 47 (17), 2268–2275.

Weaver, J.C., et al., 2012. The Stomatopod Dactyl Club: a formidable damage-tolerant biological hammer. Science 336 (6086), 1275–1280.

Wegst, U.G.K., Ashby, M.F., 2004. The mechanical efficiency of natural materials. Philos. Mag. 84 (21), 2167–2186.

Yang, W., et al., 2013a. Natural flexible dermal armor. Adv. Mater. 25 (1), 31–48.

Yang, W., et al., 2013b. Structure and fracture resistance of alligator gar (*Atractosteus spatula*) armored fish scales. Acta Biomater. 9 (4), 5876–5889.

Zhu, D., et al., 2013. Puncture resistance of the scaled skin from striped bass: collective mechanisms and inspiration for new flexible armor designs. J. Mech. Behav. Biomed. Mater. 24, 30–40.
Zhu, D.J., et al., 2012. Structure and mechanical performance of a "modern" fish scale. Adv. Eng. Mater. 14 (4), B185–B194.
Zimmermann, E.A., et al., 2013. Mechanical adaptability of the Bouligand-type structure in natural dermal armour. Nat. Commun., 4.
Zok, F.W., 2006. Developments in oxide fiber composites. J. Am. Ceram. Soc. 89 (11), 3309–3324.